ISSN: 1392-6292/ eISSN: 1648-3510

VILNIUS TECH
Vilnius Gediminas Technical University

MATHEMATICAL MODELLING and ANALYSIS

2026
Volume 31
Issue 1
Pages 26–46
https://doi.org/10.3846/mma.2026.22256

A uniformly accurate hybrid difference approximation of a system of singularly perturbed reaction-diffusion equations with delay using grid equidistribution

Aditya Kaushik[a], Shivani Jain[a] and Manju Sharma ✉ [b]

[a] *Department of Applied Mathematics, Delhi Technological University, Delhi, India*
[b] *Department of Mathematics, Indraprastha College for Women, University of Delhi, Delhi, India*

Article History:

- received September 20, 2024
- revised February 15, 2025
- accepted March 11, 2025

Abstract. This paper presents a uniformly accurate difference approximation for a system of singularly perturbed reaction-diffusion equations with delay. The proposed method utilizes an appropriate combination of exponential and cubic spline difference schemes. It employs grid equidistribution to address the challenges posed by the multiscale nature of these systems, which often feature sharp gradients and boundary layers. The grid is generated based on the equidistribution of a positive monitor function, a linear combination of a constant floor and a power of the second derivative of the solution. By using adaptive mesh generation and a spline difference method, the approach enhances the accuracy of the numerical solutions while maintaining computational efficiency. Numerical experiments validate the uniform convergence and theoretical findings, demonstrating the method's robustness irrespective of the perturbation parameter size.

Keywords: singular perturbation; reaction-diffusion equations; adaptive mesh generation; spline difference method.

AMS Subject Classification: 34BXX; 65LXX; 65QXX.

✉ Corresponding author. E-mail: manjusharma@ip.du.ac.in

1 Introduction

A singularly perturbed system of reaction-diffusion equations represents a class of mathematical models that describe the dynamics of phenomena where diffusion and reaction processes occur simultaneously but at significantly different rates. These systems are characterised by having one or more small parameters relative to others, resulting in multiscale behaviour. In such systems, the diffusion term dominates at one scale, while the reaction term dominates at

another, leading to intricate phenomena such as boundary layer formation and sharp transition regions [26]. Singularly perturbed systems find applications in various fields, including biology [24], chemistry [23], physics [6], and engineering [21], where understanding the intricate interplay between diffusion and reaction is crucial to accurately predict system behaviour.

The analysis and solution of these systems often require specialised mathematical techniques, such as asymptotic analysis and numerical methods tailored to handle stiffness and boundary layer phenomena. Although asymptotic and numerical methods offer valuable tools for tackling singularly perturbed systems of reaction-diffusion equations, they also have limitations that must be considered [25]. Asymptotic methods, such as matched asymptotic expansions, can struggle to provide accurate solutions in regions where multiple lengths or time scales interact [15]. This leads to challenges in identifying appropriate asymptotic expansions or neglecting important terms. Additionally, these methods often rely on analytical approximations, which may not capture the full complexity of the system's behaviour. Although numerical methods are valuable tools for approximating solutions to singularly perturbed reaction-diffusion systems, they have limitations when applied to uniform meshes [20]. Uniform meshes allocate grid points evenly across the domain, resulting in a constant mesh spacing that may be inadequate for resolving regions where sharp changes in the solution occur due to the scale disparity. The numerical methods on uniform meshes require excessively fine meshes to accurately capture the behaviour within the boundary layers, leading to computationally expensive simulations [20]. Moreover, using uniform meshes can exacerbate stability and convergence issues, particularly for stiff systems or when discontinuities are present, as the numerical schemes struggle to adapt to the local variations in the solution. Although uniform meshes offer simplicity and ease of implementation, they may not provide sufficiently accurate results for singularly perturbed systems without imposing a significant computational burden.

Adaptive mesh refinement techniques address this challenge by automatically increasing the mesh resolution in regions where it is needed most, such as near steep gradients or boundary layers, while maintaining coarser grids in smoother areas [3, 20]. This adaptive approach not only enhances the accuracy of the solution, but also reduces computational costs by concentrating computational resources where they are most needed. As a result, adaptive meshes enable more efficient and accurate simulations of singularly perturbed systems, making them indispensable tools for researchers and practitioners studying these complex phenomena [3, 20]. The meshes are often classified into a priori meshes and posterior meshes. A priori mesh refinement is typically based on analytical considerations or prior knowledge of the problem's characteristics. It is often used when the problem's features are well understood or when computational resources are limited. A posteriori mesh refinement, on the other hand, involves dynamically adjusting the mesh resolution during or after the solution process based on error estimates or solution properties. A posteriori meshes are particularly useful for singularly perturbed problems. Initially proposed by Bakhvalov [2], these meshes have since been extensively studied, particularly in the context of convection-diffusion problems. Notable contribu-

tions include Shishkin's piecewise equidistant meshes [20], meshes employing the equidistribution principle [8, 9, 30], Gartland-type meshes [7], Bakhvalov-Shishkin meshes [7], and Vulanović improved Shishkin meshes [34]. Further advances have led to the development of layer-adapted meshes through recursive formulations, such as Gartland-Shishkin meshes and graded meshes analysed in various studies [1, 4, 13, 14, 18, 28, 31, 32] and references therein.

The analysis of significant methods for the coupled system of singular perturbation problems based on equidistributed grids has seen little development and lacks due attention. Researchers have applied algorithms based on equidistribution principles to a wide range of practical problems, but they have conducted very little theoretical analysis to explain their success. This is primarily due to the inherent nonlinear nature of adaptive methods. For standard difference schemes, many authors [17, 19] have considered discrete analogues of the arc-length monitor function to obtain an accurate approximate solution in the context of convection-diffusion and reaction-diffusion problems. However, the authors in [16] demonstrated that an arc-length monitor function fails to produce a satisfactory numerical approximation for reaction-diffusion problems. Selecting an optimal monitor function is essentially based on the numerical discretization used, the norm of the error to be minimized, and the nature of the problem.

In this study, we extend the idea of adaptive grid generation based on the equidistribution of a positive monitor function that is a linear combination of a constant floor and a power of the second derivative of the solution to solve a coupled system of singularly perturbed delay reaction-diffusion boundary value problems and present a higher-order hybrid approximation using splines. The analysis shows that the accuracy of the numerical approximation is insensitive to the size of the singular perturbation parameter and provides insight into the convergence behavior on such grids. Numerical results are given that confirm the uniform convergence rates and the theoretical findings.

2 Continuous problem

Consider the system of singularly perturbed reaction-diffusion equations with a shift given below

$$\begin{cases} \boldsymbol{L}\wp(\varsigma): & = -\epsilon\wp''(\varsigma) + \mathbf{A}\wp(\varsigma) + \boldsymbol{B}\wp(\varsigma-\delta) = \boldsymbol{g}(\varsigma),\ \varsigma \in \Omega = (0,1), \\ \wp(\varsigma) & = \boldsymbol{\rho}(\varsigma),\ \varsigma \in [-\delta, 0], \quad \wp(1) = \boldsymbol{l}, \end{cases} \tag{2.1}$$

where $0 < \epsilon \ll 1$ is the perturbation parameter and δ denotes the small shift of order $o(\epsilon)$. Here, $\wp(\varsigma) = (\wp_1(\varsigma), \wp_2(\varsigma))^T$, $\boldsymbol{A} = (a_{mt}(\varsigma))_{2\times 2}$ is an L_0-matrix, $\boldsymbol{B} = diag(b_1(\varsigma), b_2(\varsigma))$ is a diagonal matrix. The source vector $\boldsymbol{g}(\varsigma) = (g_1(\varsigma), g_2(\varsigma))^T$ and the given data $a_{mt}(\cdot)$, $b_m(\cdot)$ and $\boldsymbol{\rho}(\varsigma) = (\rho_1(\varsigma), \rho_2(\varsigma))^T$ are sufficiently smooth functions defined on $\bar{\Omega}$. Besides, for $m, t = 1, 2$

$$a_{mm} > 0,\ b_m > 0,\ \min\left\{\left\|\frac{a_{mt}}{a_{mm}+b_m}\right\|, \left\|\frac{a_{mt}}{b_m}\right\|\right\} < 1,\ a_{mt} \le 0\ \forall\ m \ne t. \tag{2.2}$$

Since δ is of order $o(\epsilon)$, the Taylor's series expansion of $\boldsymbol{\wp}(\varsigma-\delta)$ after neglecting the higher order derivative terms in (2.1) leads to

$$\begin{cases} \boldsymbol{L}\boldsymbol{\wp}(\varsigma): & = -\epsilon\boldsymbol{\wp}''(\varsigma) - \delta\boldsymbol{B}\boldsymbol{\wp}'(\varsigma) + (\mathbf{A}+\mathbf{B})\boldsymbol{\wp}(\varsigma) = \boldsymbol{g}(\varsigma), \\ \boldsymbol{\wp}(0) & = \boldsymbol{\rho}(0) = \boldsymbol{\rho}, \quad \boldsymbol{\wp}(1) = \boldsymbol{l}, \end{cases}$$

where $\|.\|$ represents the maximum norm on Ω. The hypotheses above assures that the problem (2.1) admit a unique solution $\boldsymbol{\wp} = (\wp_1, \wp_2)^T \in \left(C^2(\Omega)\cap C(\bar{\Omega})\right)$ [20].

3 Properties of the solution

In this section, we concentrate on the stability property of the analytical solution $\boldsymbol{\wp}$ that can be derived from the maximum principle as in [29]. The differential operator $\boldsymbol{L} = (L_1, L_2)^T$ satisfies the maximum principle.

Lemma 1. *Let $\boldsymbol{L}\boldsymbol{\wp} \geq 0$ on Ω and $\boldsymbol{\wp}(0) \geq 0$, $\boldsymbol{\wp}(1) \geq 0$. Then, $\boldsymbol{\wp}(\varsigma) \geq 0$ on $\bar{\Omega}$.*

As an immediate consequence of the maximum principle, it is straightforward to obtain the following estimate.

Lemma 2. *Let $\boldsymbol{\wp}(\varsigma)$ be any smooth function. Then,*

$$\left\|\boldsymbol{\wp}(\varsigma)\right\| \leq \max\{\left\|\boldsymbol{\wp}(0)\right\|, \left\|\boldsymbol{\wp}(1)\right\|, \max_{\varsigma\in\bar{\Omega}}\|L_1\boldsymbol{\wp}\|, \max_{\varsigma\in\bar{\Omega}}\|L_2\boldsymbol{\wp}\|\}, \ \forall\, \varsigma\in\bar{\Omega}.$$

Utilising the stability property of the scalar differential operator, we proceed to estimate the stability of the operator $\boldsymbol{L}$ in the following lemma.

Lemma 3. *Let $\boldsymbol{\wp}$ be the solution of (2.1) and (2.2) holds on $\bar{\Omega}$. Then,*

$$\|\wp_m\| \leq \sum_{t=1}^{2}(\boldsymbol{\Gamma}^{-1})_{mt}\min\left\{\left\|\frac{g_t}{a_{tt}+b_t}\right\|, \left\|\frac{g_t}{b_t}\right\|\right\}, \ m=1,2,$$

where $\boldsymbol{\Gamma} = (\gamma_{mt})_{2\times 2}$ such that $\gamma_{mm}=1$, $\gamma_{mt} = -\min\left\{\left\|\frac{a_{mt}}{a_{mm}+b_m}\right\|, \left\|\frac{a_{mt}}{b_m}\right\|\right\}$ for $m\neq t$.

Proof. Let $\boldsymbol{\wp} := \boldsymbol{u}+\boldsymbol{v}$ where the components $\boldsymbol{u}$ and $\boldsymbol{v}$ satisfy

$$-\epsilon u_m'' - \delta b_m u_m' + (a_{mm}+b_m)u_m = g_m \text{ on } \Omega, \ u_m(0)=\rho_m, \ u_m(1)=l_m \text{ and}$$

$$-\epsilon v_m'' - \delta b_m v_m' + (a_{mm}+b_m)v_m = -\sum_{\substack{t=1\\ t\neq m}}^{2} a_{mt}\wp_t \text{ on } \Omega, v_m(0)=0, v_m(1)=0.$$

Lemma 2 and the triangle inequality leads to

$$\|\wp_m\| - \sum_{\substack{t=1\\ t\neq m}}^{2}\min\left\{\left\|\frac{a_{mt}}{a_{mm}+b_m}\right\|, \left\|\frac{a_{mt}}{b_m}\right\|\right\}\|\wp_t\| \leq \min\left\{\left\|\frac{g_m}{a_{mm}+b_m}\right\|, \left\|\frac{g_m}{b_m}\right\|\right\}.$$

Since, matrix $\boldsymbol{A}$ and $\boldsymbol{B}$ satisfies (2.2), the matrix $\boldsymbol{\Gamma} = (\gamma_{mt})_{2\times 2}$ is a diagonally dominant L_0-matrix. Hence, $\boldsymbol{\Gamma}$ is inverse monotone and

$$\|\wp_m\| \leq \sum_{t=1}^{2} (\boldsymbol{\Gamma}^{-1})_{mt} \min\left\{ \left\| \frac{g_t}{a_{tt}+b_t} \right\|, \left\| \frac{g_t}{b_t} \right\| \right\},\ m = 1, 2.$$

□

Next, to facilitate the analysis of the numerical discretization of (2.1), we establish derivative bounds on the solution $\boldsymbol{\wp}$ in the following lemma.

Lemma 4. *Let $\xi \in (0,1) \subset \mathbb{R}$ be such that*

$$\sum_{\substack{t=1 \\ t\neq m}}^{2} \min\left\{ \left\| \frac{a_{mt}}{a_{mm}+b_m} \right\|, \left\| \frac{a_{mt}}{b_m} \right\| \right\} < \xi < 1$$

for $m = 1, 2$. Then, for $k = 0, \ldots, 4$, $\boldsymbol{\wp}$ satisfies

$$|\wp_m^{(k)}(\varsigma)| \leq C\Big(1 + \epsilon^{-\frac{k}{2}}\Big(e^{\left(-\varsigma\sqrt{\frac{\varsigma}{\epsilon}}\right)} + e^{\left(-(1-\varsigma)\sqrt{\frac{\varsigma}{\epsilon}}\right)}\Big)\Big),\ \forall\, \varsigma \in \bar{\Omega},$$

where $\zeta = \zeta(\xi) := (1-\xi) \min\limits_{m=1,2} \min\limits_{\varsigma\in[0,1]} (a_{mm}(\varsigma) + b_m(\varsigma)) > 0$.

Proof. Proof imitates steps as in Lemma 2.4 of [12]. □

4 Solution decomposition

The standard decomposition of the solution plays a crucial role in the convergence analysis of numerical methods for singularly perturbed problems. Therefore, we decompose the solution of (2.1) into smooth and layer parts as $\boldsymbol{\wp} = \boldsymbol{u} + \boldsymbol{v}$. where the smooth component $\boldsymbol{u} = (u_1, u_2)^T$ satisfy

$$\boldsymbol{L}\boldsymbol{u}(\varsigma) = \boldsymbol{g}(\varsigma),\ \varsigma \in \Omega;\ \boldsymbol{u}(0) = \boldsymbol{u}_0(0),\ \boldsymbol{u}(1) = \boldsymbol{u}_0(1) \tag{4.1}$$

and the layer part $\boldsymbol{v} = (v_1, v_2)^T$ satisfy

$$\boldsymbol{L}\boldsymbol{v}(\varsigma) = 0,\ \varsigma \in \Omega;\ \boldsymbol{v}(0) = \boldsymbol{\rho} - \boldsymbol{u}_0(0),\ \boldsymbol{v}(1) = \boldsymbol{l} - \boldsymbol{u}_0(1). \tag{4.2}$$

Following this, we utilize a proposition from [27] stated below and the standard factorization to estimate precise bounds on the components and their derivatives.

Proposition 1. *Let $\theta > 0$ and $I = [\lambda, \lambda+\theta]$ be an arbitrary interval. If $F \in C^2(I)$, then,*

$$\|F'\|_I \leq \frac{2}{\theta}\|F\|_I + \frac{\theta}{2}\|F''\|_I.$$

Lemma 5. *Let* $\boldsymbol{\wp} := \boldsymbol{u} + \boldsymbol{v}$ *be the solution of* (2.1) *where* $\boldsymbol{u}$ *and* $\boldsymbol{v}$ *satisfy* (4.1) *and* (4.2)*, respectively. Then, the smooth part* $\boldsymbol{u} = (u_1, u_2)^T$ *satisfies*

$$\left\| u_m^{(k)} \right\| \leq C\Big(1+\epsilon^{\frac{(2-k)}{2}}\Big),\ k = 0, ..., 4,\ m = 1, 2,$$

and the layer part $\boldsymbol{v} = (v_1, v_2)^T$ satisfies

$$\left\| v_m^k \right\| \leq C\Big(1+\epsilon^{-\frac{k}{2}}\Big(e^{\left(-\varsigma\sqrt{\frac{\varsigma}{\epsilon}}\right)}+e^{\left(-(1-\varsigma)\sqrt{\frac{\varsigma}{\epsilon}}\right)}\Big)\Big),\ k=0, ..., 4,\ m = 1, 2,\ \zeta \in \bar{\Omega}.$$

Proof. Proof imitates steps as in Lemma 3 and Lemma 4 of [22], Lemma 2.2 of [5] and Lemma 2.6 of [12].
□

5 Grid structure

The development of the adaptive numerical method relies on a solution adaptive moving mesh algorithm that automatically identifies the basic characteristics of the boundary layers through an equidistribution principle. Following [10,11], we consider the monitor function

$$M = \beta + |v_1''|^{\frac{1}{2}} + |v_2''|^{\frac{1}{2}}, \tag{5.1}$$

where v_1 and v_2 are the layer components of the solution $\boldsymbol{\wp} = (\wp_1, \wp_2)^T$ and β is a positive constant. Earlier works [8,10,11] show that one should choose the least value of monitor function with caution to improve convergence. Therefore, by setting an appropriate floor value β, the grid prevents point clustering within layers and ensures proper distribution of grid points outside layers.

Using the derivative bounds for $v(\varsigma)$ in Lemma (5) yields an approximation of $v_m''(\varsigma)$, $m = 1, 2$ at $\varsigma = \varsigma_t$ given by

$$v_m''(\varsigma) = \begin{cases} \dfrac{\alpha_0}{\epsilon} \exp\Big(-\varsigma\sqrt{\zeta/\epsilon}\Big), & \varsigma \in [0, \frac{1}{2}], \\ \dfrac{\alpha_1}{\epsilon} \exp\Big(-(1-\varsigma)\sqrt{\zeta/\epsilon}\Big), & \varsigma \in \big(\frac{1}{2}, 1\big], \end{cases}$$

where α_0 and α_1 are the constants. Imitating the analysis from [9, 10, 11], we have

$$\int_0^1 (|v_1''|^{\frac{1}{2}} + |v_2''|^{\frac{1}{2}}) d\varsigma \equiv \gamma \approx \frac{2}{\sqrt{\zeta}}(|\alpha_0|^{\frac{1}{2}} + |\alpha_1|^{\frac{1}{2}}).$$

Now, using (5.1) to obtain a map

$$\begin{aligned} &\frac{\beta}{\gamma}\varsigma(\xi) + \theta_0\Big(1 - \exp\Big(-\frac{\varsigma(\xi)}{2}\sqrt{\frac{\zeta}{\epsilon}}\Big)\Big) = \xi\big(\beta/\gamma + 1\big),\ \ \varsigma(\xi) \leq \frac{1}{2} \\ &\frac{\beta}{\gamma}(1-\varsigma(\xi))+\theta_1\Big(1-\exp\Big(-\frac{(1-\varsigma(\xi))}{2}\sqrt{\frac{\zeta}{\epsilon}}\Big)\Big)=(1-\xi)\big(\beta/\gamma+1\big),\ \ \varsigma(\xi) > \frac{1}{2}, \end{aligned} \tag{5.2}$$

where $\theta_0 = \frac{|\alpha_0|^{\frac{1}{2}}}{|\alpha_0|^{\frac{1}{2}}+|\alpha_1|^{\frac{1}{2}}}$ and $\theta_1 = \frac{|\alpha_1|^{\frac{1}{2}}}{|\alpha_0|^{\frac{1}{2}}+|\alpha_1|^{\frac{1}{2}}} = 1-\theta_0$.

Given the relation between adaptive grid $\{\varsigma_t\}_{t=0}^{N}$ and uniform grid $\left\{\xi_t = \frac{t}{N}\right\}_{t=0}^{N}$, the required non-uniform grid is given by

$$\frac{\beta}{\gamma}\varsigma_t + \theta_0\left(1 - e^{\left(-\frac{\varsigma_t}{2}\sqrt{\frac{\zeta}{\epsilon}}\right)}\right) = \frac{t}{N}\left(\frac{\beta}{\gamma}+1\right), \ \ \varsigma_t \le \frac{1}{2} \tag{5.3}$$

$$\frac{\beta}{\gamma}(1-\varsigma_t) + \theta_1\left(1 - e^{\left(-\frac{(1-\varsigma_t)}{2}\sqrt{\frac{\zeta}{\epsilon}}\right)}\right) = \left(1-\frac{t}{N}\right)\left(\frac{\beta}{\gamma}+1\right), \ \ \varsigma_t > \frac{1}{2}. \tag{5.4}$$

Next, for an appropriate β, we study the structure of the grid so generated, some of the associated properties and illustrate its distribution.

Lemma 6. *Let $\beta = \gamma$. Then,*

$$\varsigma_{k_l} < 2\sqrt{\frac{\epsilon}{\zeta}}\log N < \varsigma_{k_{l+1}} \text{ and } \varsigma_{k_{r-1}} < 1 - 2\sqrt{\frac{\epsilon}{\zeta}}\log N < \varsigma_{k_r},$$

where

$$k_l = \left[\frac{\theta_0}{2}(N-1) + \sqrt{\frac{\epsilon}{\zeta}}N\log N\right], \ \ k_r = \left[N - \left(\frac{\theta_1}{2}(N-1) + \sqrt{\frac{\epsilon}{\zeta}}N\log N\right)\right] + 1.$$

Here, $[\cdot]$ represents the integral part of the term. Moreover,

$$e^{\left(-\frac{\varsigma_t}{2}\sqrt{\frac{\zeta}{\epsilon}}\right)} \le CN^{-1}, \ t \ge k_l - 1, \ \varsigma_t \le \frac{1}{2},$$
$$e^{\left(-\frac{(1-\varsigma_t)}{2}\sqrt{\frac{\zeta}{\epsilon}}\right)} \le CN^{-1}, \ t \le k_r, \ \varsigma_t > \frac{1}{2}.$$

Proof. Put $\varsigma_t = 2\sqrt{\frac{\epsilon}{\zeta}}\log N$ in (5.3) and solve for t to find k_l. Using (5.4) we can similarly compute k_r. □

Setting $\beta = \gamma$ aligns the equidistributed grid with some features of the a priori mesh. However, the exponential stretching within layers reduces discretisation errors, enhancing accuracy [9, 11]. Next, we obtain bounds on the grid width in the layer region $\left(\{\varsigma_t\}_{t=0}^{k_l-1}\right.$ and $\left.\{\varsigma_t\}_{t=k_r+1}^{N}\right)$ and the outer region $\left(\{\varsigma_t\}_{t=k_l}^{k_r}\right)$.

Lemma 7. *For $t=\{1,...,k_l\} \cup \{k_r+1,...,N\}$, $\hbar_t := \hbar_t - \hbar_{t-1} < 2C\sqrt{\epsilon}/\zeta$. Moreover,*

$$|\hbar_{t+1} - \hbar_t| \le \begin{cases} C\hbar_t^2, & t = 1,...,k_l-1, \\ C\hbar_{t+1}^2, & t = k_r+1,...,N-1. \end{cases}$$

Proof. We estimate the result for the left layer. The result for the right layer portion follows analogously. Imitating the steps from [11, Lemma 3.2] we use (5.3) to obtain $\bar{\varsigma_t} > \varsigma_t$ such that $e^{\left(-\frac{\varsigma_t}{2}\sqrt{\frac{\zeta}{\epsilon}}\right)} = 1 - \frac{2t}{\theta_0 N}$. A rearrangement of

terms yields $\varsigma_t < \bar{\varsigma}_t = -2\sqrt{\frac{\epsilon}{\zeta}}\log\left(1-\frac{2t}{\theta_0 N}\right)$. Using $\bar{\varsigma}_t$ into (5.3) to compute

$$\varsigma_t > \underline{\varsigma_t} = -2\sqrt{\frac{\epsilon}{\zeta}}\left(1-\frac{1}{\theta_0}\left(\frac{2t}{N}+2\sqrt{\frac{\epsilon}{\zeta}}\log\left(1-\frac{2t}{\theta_0 N}\right)\right)\right).$$

Thus, for $t = 1, ..., k_l$

$$\hbar_t = \varsigma_t - \varsigma_{t-1} < \bar{\varsigma}_t - \varsigma_{t-1} = 2\sqrt{\frac{\epsilon}{\zeta}}\log\left[1+\frac{2+2\sqrt{\frac{\zeta}{\epsilon}}N\log\left(\frac{\theta_0 N}{\theta_0 N-2(t-1)}\right)}{\theta_0 N-2t}\right] < 2C\sqrt{\frac{\epsilon}{\zeta}}.$$

Moreover, note that

$$\frac{|\hbar_{t+1}-\hbar_t|}{\hbar_t^2} \le \frac{2\left|\varsigma_{\xi\xi}\left(\phi_t^{(1)}\right)\right|}{\left(\varsigma_\xi\left(\phi_t^{(2)}\right)\right)^2}, \text{ where } \phi_t^{(1)} \in (\xi_{t-1},\xi_{t+1}), \;\; \phi_t^{(2)} \in (\xi_{t-1},\xi_t).$$

Then, from (5.2) and $\beta = \gamma$, we obtain

$$\varsigma_\xi(\phi) = \frac{4\sqrt{\frac{\epsilon}{\zeta}}}{2\sqrt{\frac{\epsilon}{\zeta}}+\theta_0 e^{\left(-\frac{\varsigma(\phi)}{2}\sqrt{\frac{\zeta}{\epsilon}}\right)}} \text{ and } \varsigma_{\xi\xi}(\phi) = \frac{8\theta_0\sqrt{\frac{\epsilon}{\zeta}}e^{\left(-\frac{\varsigma(\phi)}{2}\sqrt{\frac{\zeta}{\epsilon}}\right)}}{\left(2\frac{\epsilon}{\zeta}+\theta_0 e^{\left(-\frac{\varsigma(\phi)}{2}\sqrt{\frac{\zeta}{\epsilon}}\right)}\right)^3}.$$

This implies that

$$\frac{|\hbar_{t+1}-\hbar_t|}{\hbar_t^2} \le \frac{\theta_0\sqrt{\frac{\zeta}{\epsilon}}\left(2\frac{\zeta}{\epsilon}+\theta_0 e^{\left(-\frac{\varsigma(\phi)}{2}\sqrt{\frac{\zeta}{\epsilon}}\right)}\right)^2}{2\left(2\frac{\zeta}{\epsilon}+\theta_0\exp\left(-\frac{\varsigma(\phi)}{2}\sqrt{\frac{\zeta}{\epsilon}}\right)\right)^3} \le C.$$

□

Next, we find the following generalized bounds on $\hbar_t$.

Lemma 8. *For $t = 1, ..., N$, the adaptive grid width satisfies $\hbar_t \le CN^{-1}$.*

Proof. For proof, see Lemma 2.4 of [12]. □

6 The difference method

We now describe the difference approximation of (2.1) on the adaptive grid $\bar{\Omega}_E^N \equiv \{0 = \varsigma_0 < \varsigma_1 < \cdots < \varsigma_N = 1\}$. We employ a cubic spline difference method within the boundary layer region and an exponential spline difference method in the outer layer region.

The cubic spline polynomials $S_m(\varsigma)$ for $m = 1, 2$, are determined by solving $D^4 S_m(\varsigma) = 0$, for all $\varsigma \in [\varsigma_{t-1}, \varsigma_t]$, $t = 1, 2, \ldots N$ such that $S_m(\varsigma_{t-1}) =$

$Y_m(\varsigma_{t-1})$, $S_m(\varsigma_t) = Y_m(\varsigma_t)$, $S''_m(\varsigma_{t-1}) = Y''_m(\varsigma_{t-1})$ and $S''_m(\varsigma_t) = Y''_m(\varsigma_t)$. Now, for $t = 0, \ldots, N$, we use $S''_m(\varsigma_t) = \mathcal{M}_{m,t}$ to find

$$S_m(\varsigma) = \frac{(\varsigma_t-\varsigma)^3}{6\hbar_t}\mathcal{M}_{m,t-1} + \frac{(\varsigma-\varsigma_{t-1})^3}{6\hbar_t} + \Big(Y_m(\varsigma_{t-1}) - \frac{\hbar_t^2}{6}\mathcal{M}_{m,t-1}\Big)\frac{(\varsigma_t-\varsigma)}{\hbar_t} + \Big(Y_m(\varsigma_t) - \frac{\hbar_t^2}{6}\mathcal{M}_{m,t}\Big)\frac{(\varsigma-\varsigma_{t-1})}{\hbar_t}.$$

For $t = 1, ..., N-1$, the continuity constraint of $S'_m(\varsigma)$ at ς_t, leads to the following system for $\mathcal{M}_{m,t}$

$$\frac{\hbar_t}{6}\mathcal{M}_{m,t-1} + \Big(\frac{\hbar_t+\hbar_{t+1}}{3}\Big)\mathcal{M}_{m,t} + \frac{\hbar_{t+1}}{6}\mathcal{M}_{m,t+1} = \frac{Y_m(\varsigma_{t+1}) - Y_m(\varsigma_t)}{\hbar_{t+1}} - \frac{Y_m(\varsigma_t) - Y_m(\varsigma_{t-1})}{\hbar_t}. \tag{6.1}$$

To obtain second order approximation for $Y'_m(\varsigma)$, we use Taylor's series expansion of Y_m about ς_t. Consequently, for $m = 1, 2$, we obtain

$$Y'_m(\varsigma_t) \approx \frac{\hbar_t^2 Y_m(\varsigma_{t+1}) + (\hbar_{t+1}^2 - \hbar_t^2)Y_m(\varsigma_t) - \hbar_{t+1}^2 Y_m(\varsigma_{t-1})}{\hbar_{t+1}\hbar_t(\hbar_{t+1}+\hbar_t)}$$
$$Y''_m(\varsigma_t) \approx \frac{2(\hbar_t Y_m(\varsigma_{t+1}) - (\hbar_{t+1}+\hbar_t)Y_m(\varsigma_t) + \hbar_{t+1}Y_m(\varsigma_{t-1}))}{\hbar_{t+1}\hbar_t(\hbar_{t+1}+\hbar_t)}.$$

A substitution in $Y'_m(\varsigma_{t+1}) \approx Y'_m(\varsigma_t) + \hbar_{t+1}Y''_m(\varsigma_t)$ and $Y'_m(\varsigma_{t-1}) \approx Y'_m(\varsigma_t) - \hbar_t Y''_m(\varsigma_t)$ leads to

$$Y'_m(\varsigma_{t+1}) \approx \frac{(\hbar_t^2 + 2\hbar_{t+1}\hbar_t)Y_m(\varsigma_{t+1}) - (\hbar_{t+1}+\hbar_t)^2 Y_m(\varsigma_t) + \hbar_{t+1}^2 Y_m(\varsigma_{t-1})}{\hbar_{t+1}\hbar_t(\hbar_{t+1}+\hbar_t)}$$
$$Y'_m(\varsigma_{t-1}) \approx \frac{2(-\hbar_t^2 Y_m(\varsigma_{t+1}) + (\hbar_{t+1}+\hbar_t)^2 Y_m(\varsigma_t) - (\hbar_{t+1}^2 + 2\hbar_{t+1}\hbar_t)Y_m(\varsigma_{t-1}))}{\hbar_{t+1}\hbar_t(\hbar_{t+1}+\hbar_t)}.$$

Substitute $\mathcal{M}_{m,t}$ for $i = t, t \pm 1$, from

$$-\epsilon\mathcal{M}_{1,i} - \delta b_1(\varsigma_i)Y'_1(\varsigma_i) + (a_{11}(\varsigma_i) + b_1(\varsigma_i))Y_1(\varsigma_i) + a_{12}(\varsigma_i)Y_2(\varsigma_i) = g_1(\varsigma_i),$$
$$-\epsilon\mathcal{M}_{2,i} - \delta b_2(\varsigma_i)Y'_2(\varsigma_i) + a_{21}(\varsigma_i)Y_1(\varsigma_i) + (a_{22}(\varsigma_i) + b_2(\varsigma_i))Y_2(\varsigma_i) = g_2(\varsigma_i)$$

in (6.1), we get the following system for $t = 1, ...N-1$, $m = 1, 2$,

$$\Big(\frac{-\epsilon}{\hbar_t(\hbar_{t+1}+\hbar_t)} + \frac{\hbar_t}{6(\hbar_{t+1}+\hbar_t)}\big(a_{mm}(\varsigma_{t-1}) + b_m(\varsigma_{t-1})\big) + \frac{\hbar_{t+1}+2\hbar_t}{6(\hbar_{t+1}+\hbar_t)^2}\delta b_m(\varsigma_{t-1}) + \frac{\hbar_{t+1}}{3\hbar_t(\hbar_{t+1}+\hbar_t)}\delta b_m(\varsigma_t) - \frac{(\hbar_{t+1})^2}{6\hbar_t(\hbar_{t+1}+\hbar_t)^2}\delta b_m(\varsigma_{t+1})\Big)Y_{m,t-1}$$
$$+\Big(\frac{\epsilon}{\hbar_{t+1}\hbar_t} + \frac{(a_{mm}(\varsigma_t) + b_m(\varsigma_t))}{3} - \frac{1}{6\hbar_{t+1}}\delta b_m(\varsigma_{t-1}) - \frac{(\hbar_{t+1}-\hbar_t)}{3\hbar_{t+1}\hbar_t}\delta b_m(\varsigma_t)$$

$$+\frac{1}{6\hbar_t}\delta b_m(\varsigma_{t+1})\Big)Y_{m,t}+\Big(\frac{-\epsilon}{\hbar_{t+1}(\hbar_{t+1}+\hbar_t)}+\frac{\hbar_{t+1}}{6(\hbar_{t+1}+\hbar_t)}(a_{mm}(\varsigma_{t+1})+b_m(\varsigma_{t+1}))$$
$$+\frac{(\hbar_t)^2}{6(\hbar_{t+1}+\hbar_t)^2}\delta b_m(\varsigma_{t-1})-\frac{\hbar_t}{3\hbar_{t+1}(\hbar_{t+1}+\hbar_t)}\delta b_m(\varsigma_t)$$
$$-\frac{(\hbar_t+2\hbar_{t+1})}{6(\hbar_{t+1}+\hbar_t)^2}\delta b_m(\varsigma_{t+1})\Big)Y_{m,t+1}+\Big(\frac{\hbar_t}{6(\hbar_{t+1}+\hbar_t)}a_{m(3-m)}(\varsigma_{t-1})\Big)Y_{(3-m),t-1}$$
$$+\Big(\frac{a_{m(3-m)}(\varsigma_t)}{3}\Big)Y_{(3-m),t}+\Big(\frac{\hbar_{t+1}}{6(\hbar_{t+1}+\hbar_t)}a_{m(3-m)}(\varsigma_{t+1})\Big)Y_{(3-m),t+1}$$
$$=\frac{\hbar_t}{6(\hbar_{t+1}+\hbar_t)}g_m(\varsigma_{t-1})+\frac{g_m(\varsigma_t)}{3}+\frac{\hbar_{t+1}}{6(\hbar_{t+1}+\hbar_t)}g_m(\varsigma_{t+1}).$$

In a similar way, we devise an exponential difference scheme for an outer solution.

The exponential spline is determined by solving

$$\begin{cases}(D^4-p_{m,t}^2D^2)T_m=0,\ \forall\varsigma\in[\varsigma_{t-1},\varsigma_t],\ m=1,2,\ t=1,...,N,\\ T_m(\varsigma_{t-1})=Y_m(\varsigma_{t-1}),\ T_m(\varsigma_t)=Y(\varsigma_t),\ T_m''(\varsigma_{t-1})=T_{m,t-1}'',\ T_m''(\varsigma_t)=T_{m,t}'',\end{cases}$$

where $p_{m,t}$ are tension parameters. As in our earlier derivation, we employ continuity constraints to derive a system of equations representing the exponential spline relation

$$\begin{cases}e_{m,t}T_{m,t-1}''+(d_{m,t}+d_{m,t+1})T_{m,t}''+e_{m,t+1}T_{m,t+1}''\\ \quad=\dfrac{Y_m(\varsigma_{t+1})-Y_m(\varsigma_t)}{\hbar_{t+1}}-\dfrac{Y_m(\varsigma_t)-Y_m(\varsigma_{t-1})}{\hbar_t},\\ e_{m,t}=\dfrac{s_{m,t}-p_{m,t}\hbar_t}{p_{m,t}^2s_{m,t}\hbar_t},\ d_{m,t}=\dfrac{p_{m,t}\hbar_tc_{m,t}-s_{m,t}}{p_{m,t}^2s_{m,t}\hbar_t},\\ s_{m,t}=\sinh(p_{m,t}\hbar_t),\ c_{m,t}=\cosh(p_{m,t}\hbar_t).\end{cases}\tag{6.2}$$

Now substitute $T_{m,t}''$ for $i=t,t\pm1$, from

$$-\epsilon T_{1,i}''-\delta b_1(\varsigma_i)Y_1'(\varsigma_i)+(a_{11}(\varsigma_i)+b_1(\varsigma_i))Y_1(\varsigma_i)+a_{12}(\varsigma_i)Y_2(\varsigma_i)=g_1(\varsigma_i),$$
$$-\epsilon T_{2,i}''-\delta b_2(\varsigma_i)Y_2'(\varsigma_i)+a_{21}(\varsigma_i)Y_1(\varsigma_i)+(a_{22}(\varsigma_i)+b_2(\varsigma_i))Y_2(\varsigma_i)=g_2(\varsigma_i),$$

into (6.2), we get the following system for $t=1,\dots N-1$, $m=1,2$

$$\Big(\frac{-\epsilon}{\hbar_t(\hbar_{t+1}+\hbar_t)}+\frac{e_{m,t}}{\hbar_{t+1}+\hbar_t}(a_{mm}(\varsigma_{t-1})+b_m(\varsigma_{t-1}))+\frac{e_{m,t}(\hbar_{t+1}+2\hbar_t)}{\hbar_t(\hbar_{t+1}+\hbar_t)^2}\delta b_m(\varsigma_{t-1})$$
$$+\frac{(d_{m,t}+d_{m,t+1})\hbar_{t+1}}{\hbar_t(\hbar_{t+1}+\hbar_t)^2}\delta b_m(\varsigma_t)-\frac{e_{m,t+1}\hbar_{t+1}}{\hbar_t(\hbar_{t+1}+\hbar_t)^2}\delta b_m(\varsigma_{t+1})\Big)Y_{m,t-1}$$
$$+\Big(\frac{\epsilon}{\hbar_{t+1}\hbar_t}+\Big(\frac{d_{m,t}+d_{m,t+1}}{\hbar_{t+1}+\hbar_t}\Big)(a_{mm}(\varsigma_t)+b_m(\varsigma_t))-\frac{e_{m,t}}{\hbar_{t+1}\hbar_t}\delta b_m(\varsigma_{t-1})$$
$$-\frac{(d_{m,t}+d_{m,t+1})(\hbar_{t+1}-\hbar_t)}{\hbar_{t+1}\hbar_t(h_{t+1}+\hbar_t)}\delta b_m(\varsigma_t)+\frac{e_{m,t+1}}{\hbar_{t+1}\hbar_t}\delta b_m(\varsigma_{t+1})\Big)Y_{m,t}$$
$$+\Big(\frac{-\epsilon}{\hbar_{t+1}(\hbar_{t+1}+\hbar_t)}+\frac{e_{m,t+1}}{\hbar_{t+1}+\hbar_t}(a_{mm}(\varsigma_{t+1})+b_m(\varsigma_{t+1}))+\frac{e_{m,t}\hbar_t}{\hbar_{t+1}(\hbar_{t+1}+\hbar_t)^2}$$

$$\times\delta b_m(\varsigma_{t-1})-\frac{(d_{m,t}+d_{m,t+1})\hbar_t}{\hbar_{t+1}(\hbar_{t+1}+\hbar_t)^2}\delta b_m(\varsigma_t)-\frac{e_{m,t+1}(\hbar_t+2\hbar_{t+1})}{\hbar_{t+1}(\hbar_{t+1}+\hbar_t)^2}\delta b_m(\varsigma_{t+1})\Big)Y_{m,t+1}$$
$$+\frac{e_{m,t}}{\hbar_{t+1}+\hbar_t}a_{m(3-m)}(\varsigma_{t-1})Y_{(3-m),t-1}+\left(\frac{d_{m,t}+d_{m,t+1}}{\hbar_{t+1}+\hbar_t}\right)$$
$$\times a_{m(3-m)}(\varsigma_t)Y_{(3-m),t}+\frac{e_{m,t+1}}{\hbar_{t+1}+\hbar_t}a_{m(3-m)}(\varsigma_{t+1})Y_{(3-m),t+1}$$
$$=\frac{e_{m,t}}{\hbar_{t+1}+\hbar_t}g_m(\varsigma_{t-1})+\left(\frac{d_{m,t}+d_{m,t+1}}{\hbar_{t+1}+\hbar_t}\right)g_m(\varsigma_t)+\frac{e_{m,t+1}}{\hbar_{t+1}+\hbar_t}g_m(\varsigma_{t+1}).$$

Therefore, in the outer layer portion, the proposed method mitigates the non-monotonic behaviour of the cubic spline difference method by incorporating exponential splines. Consequently, the associated problem (2.1) takes the form: Find $\boldsymbol{Y}=(Y_1,Y_2)^T$ such that

$$[\boldsymbol{L}^N\boldsymbol{Y}]_t=[\Gamma\boldsymbol{g}]_t$$
$$\iff\begin{cases}[L_1^N\boldsymbol{Y}]\equiv r^-_{1,t}Y_{1,t-1}+r^c_{1,t}Y_{1,t}+r^+_{1,t}Y_{1,t+1}+q^-_{m,t}a_{12,t-1}Y_{2,t-1}\\ \quad+q^c_{m,t}a_{12,t}Y_{2,t}+q^+_{m,t}a_{12,t+1}Y_{2,t+1}=q^-_{m,t}g_{1,t-1}+q^c_{m,t}g_{1,t}\\ \quad+q^+_{m,t}g_{1,t+1},\\ [L_2^N\boldsymbol{Y}]\equiv r^-_{2,t}Y_{2,t-1}+r^c_{2,t}Y_{2,t}+r^+_{2,t}Y_{2,t+1}+q^-_{m,t}a_{21,t-1}Y_{1,t-1}\\ \quad+q^c_{m,t}a_{21,t}Y_{1,t}+q^+_{m,t}a_{21,t+1}Y_{1,t+1}=q^-_{m,t}g_{2,t-1}+q^c_{m,t}g_{2,t}\\ \quad+q^+_{m,t}g_{2,t+1},\\ Y_{1,0}=\wp_1(0),\ Y_{1,N}=\wp_1(1),\ Y_{2,0}=\wp_2(0),\ Y_{2,N}=\wp_2(1),\end{cases}\tag{6.3}$$

where $[\Gamma(g_m)]_t=q^-_{m,t}g_{m,t-1}+q^c_{m,t}g_{m,t}+q^+_{m,t}g_{m,t+1}$, $\boldsymbol{L}^N=(L_1,L_2)^N$ and $\boldsymbol{g}_t=(g_{1,t},g_{2,t})^T$.

The values of the coefficients $r^*_{m,t}$ and $q^*_{m,t}$, where $m=1,2$, $t=1,...,N-1$ and $*=-,c,+$, are determined based on the location of the grid points ς_t that partition the domain $[0,1]$ of $\boldsymbol{L}^N$. The coefficients are given as follows:

When ς_t lies within the boundary layer part of the grid, i.e., $t\in\{1,...k_l-1\}\cup\{k_r+1,...,N-1\}$, the cubic spline difference method employed to determine the coefficients reads

$$r^-_{m,t}=\frac{-\epsilon}{\hbar_t(\hbar_{t+1}+\hbar_t)}+q^-_{m,t}(a_{mm}(\varsigma_{t-1})+b_m(\varsigma_{t-1}))+\frac{\hbar_{t+1}+2\hbar_t}{6(\hbar_{t+1}+\hbar_t)^2}\delta b_m(\varsigma_{t-1})$$
$$+\frac{\hbar_{t+1}}{3\hbar_t(\hbar_{t+1}+\hbar_t)}\delta b_m(\varsigma_t)-\frac{(\hbar_{t+1})^2}{6\hbar_t(\hbar_{t+1}+\hbar_t)^2}\delta b_m(\varsigma_{t+1}),$$
$$r^c_{m,t}=\frac{\epsilon}{\hbar_{t+1}\hbar_t}+q^c_{m,t}(a_{mm}(\varsigma_t)+b_m(\varsigma_t))-\frac{1}{6\hbar_{t+1}}\delta b_m(\varsigma_{t-1})$$
$$-\frac{(\hbar_{t+1}-\hbar_t)}{3\hbar_{t+1}\hbar_t}\delta b_m(\varsigma_t)+\frac{1}{6\hbar_t}\delta b_m(\varsigma_{t+1}),$$
$$r^+_{m,t}=\frac{-\epsilon}{\hbar_t(\hbar_{t+1}+\hbar_t)}+q^+_{m,t}(a_{mm}(\varsigma_{t+1})+b_m(\varsigma_{t+1}))+\frac{(\hbar_t)^2}{6(\hbar_{t+1}+\hbar_t)^2}$$
$$\times\delta b_m(\varsigma_{t-1})-\frac{\hbar_t}{3\hbar_{t+1}(\hbar_{t+1}+\hbar_t)}\delta b_m(\varsigma_t)-\frac{(\hbar_t+2\hbar_{t+1})}{6(\hbar_{t+1}+\hbar_t)^2}\delta b_m(\varsigma_{t+1}),$$

$$q^{-}_{m,t}=\frac{\hbar_t}{6(\hbar_{t+1}+\hbar_t)},\quad q^{c}_{m,t}=\frac{1}{3},\quad q^{+}_{m,t}=\frac{\hbar_{t+1}}{6(\hbar_{t+1}+\hbar_t)}.$$

When ς_t lies outside layers, i.e., $t\in\{k_l,\ldots,k_r\}$, the coefficients associated with the exponential spline difference method reads

$$\begin{aligned}
r^{-}_{m,t}&=\frac{-\epsilon}{\hbar_t(\hbar_{t+1}+\hbar_t)}+q^{-}_{m,t}(a_{mm}(\varsigma_{t-1})+b_m(\varsigma_{t-1}))\\
&+\frac{e_{m,t}(\hbar_{t+1}+2\hbar_t)}{\hbar_t(\hbar_{t+1}+\hbar_t)^2}\delta b_m(\varsigma_{t-1})+\frac{(d_{m,t}+d_{m,t+1})\hbar_{t+1}}{\hbar_t(\hbar_{t+1}+\hbar_t)^2}\delta b_m(\varsigma_t)\\
&-\frac{e_{m,t+1}\hbar_{t+1}}{\hbar_t(\hbar_{t+1}+\hbar_t)^2}\delta b_m(\varsigma_{t+1}),\\
r^{c}_{m,t}&=\frac{\epsilon}{\hbar_{t+1}\hbar_t}+q^{c}_{m,t}(a_{mm}(\varsigma_t)+b_m(\varsigma_t))-\frac{e_{m,t}}{\hbar_{t+1}\hbar_t}\delta b_m(\varsigma_{t-1})\\
&-\frac{(d_{m,t}+d_{m,t+1})(\hbar_{t+1}-\hbar_t)}{\hbar_{t+1}\hbar_t(h_{t+1+\hbar_t})}\delta b_m(\varsigma_t)+\frac{e_{m,t+1}}{\hbar_{t+1}\hbar_t}\delta b_m(\varsigma_{t+1}),\\
r^{+}_{m,t}&=\frac{-\epsilon}{\hbar_t(\hbar_{t+1}+\hbar_t)}+q^{+}_{m,t}(a_{mm}(\varsigma_{t+1})+b_m(\varsigma_{t+1}))\\
&+\frac{e_{m,t}\hbar_t}{\hbar_{t+1}(\hbar_{t+1}+\hbar_t)^2}\delta b_m(\varsigma_{t-1})-\frac{(d_{m,t}+d_{m,t+1})\hbar_t}{\hbar_{t+1}(\hbar_{t+1}+\hbar_t)^2}\delta b_m(\varsigma_t)\\
&-\frac{e_{m,t+1}(\hbar_t+2\hbar_{t+1})}{\hbar_{t+1}(\hbar_{t+1}+\hbar_t)^2}\delta b_m(\varsigma_{t+1}),
\end{aligned}$$

$$q^{-}_{m,t}=\frac{e_{m,t}}{\hbar_{t+1}+\hbar_t},\quad q^{+}_{m,t}=\frac{e_{m,t+1}}{\hbar_{t+1}+\hbar_t},\quad q^{c}_{m,t}=\frac{d_{m,t}}{\hbar_{t+1}+\hbar_t}+\frac{d_{m,t+1}}{\hbar_{t+1}+\hbar_t}.$$

7 Error analysis

Over the adaptive generated grid, we investigate the consistency error associated with hybrid spline difference discretization (6.3). As in Section 4, we decompose discrete approximate solution $\boldsymbol{Y}$ of (2.1) into smooth and layer parts as $\boldsymbol{Y}:=\boldsymbol{U}+\boldsymbol{V}$, where the smooth component $\boldsymbol{U}$ satisfies

$$[\boldsymbol{L}^N\boldsymbol{U}]=[\Gamma\boldsymbol{g}]_t,\ t=1,...,N-1;\ \boldsymbol{U}_0=\boldsymbol{u}(0),\ \boldsymbol{U}_N=\boldsymbol{u}(1)$$

and the boundary layer part $\boldsymbol{V}$ satisfies

$$[\boldsymbol{L}^N\boldsymbol{V}]=[\Gamma\boldsymbol{g}]_t,\ t=1,...,N-1;\ \boldsymbol{V}_0=\boldsymbol{v}(0),\ \boldsymbol{V}_N=\boldsymbol{v}(1).$$

Then, at each ς_t, the error associated with $\boldsymbol{Y}_t$ satisfies

$$\left\|\boldsymbol{Y}_t-\boldsymbol{\wp}(\varsigma_t)\right\|\le\left\|\boldsymbol{U}_t-\boldsymbol{u}(\varsigma_t)\right\|+\left\|\boldsymbol{V}_t-\boldsymbol{v}(\varsigma_t)\right\|.$$

Lemma 9. *The smooth component $\boldsymbol{u}$ of the solution $\boldsymbol{\wp}$ and its discrete approximation $\boldsymbol{U}$ satisfies*

$$\left\|\boldsymbol{L}^N(\boldsymbol{U}-\boldsymbol{u})(\varsigma_t)\right\|\le CN^{-2},\ t=1,...,N-1.$$

Proof.

1. When $t \in \{1, \ldots, k_l - 1\} \cup \{k_r + 1, \ldots, N - 1\}$, the spline difference approximation is obtained using cubic splines. Then, for $m = 1, 2$, the Taylor's expansion yields

$$\begin{aligned}\left\|\boldsymbol{L}_m^N(\boldsymbol{U}-\boldsymbol{u})(\varsigma_t)\right\| &= |(L_m - L_m^N)\boldsymbol{u}(\varsigma_t)| \\ &\leq C\epsilon|\hbar_{t+1}-\hbar_t\left\|\left|u_m'''(\varsigma)\right\|_{[\varsigma_{t-1},\varsigma_{t+1}]}+C\epsilon(\hbar_{t+1}^2+\hbar_t^2)\left\|u_m^{(iv)}(\varsigma)\right\|_{[\varsigma_t,\varsigma_{t+1}]}\right. \\ &\leq C\epsilon\hbar_t^2(1+\epsilon^{\frac{-1}{2}})+C(\hbar_{t+1}^2+\hbar_t^2) \leq C(\hbar_{t+1}^2+\hbar_t^2).\end{aligned}$$

   The required estimate follows immediately from Lemmas 5, 7 and 8.

2. When $t \in \{k_l, \ldots, k_r\}$, the spline difference approximation is obtained using exponential splines. Then, it is easy to follow that

$$\left\|\boldsymbol{L}_m^N(\boldsymbol{U}-\boldsymbol{u})(\varsigma_t)\right\| = |(L_m - L_m^N)\boldsymbol{u}(\varsigma_t)| \leq C\epsilon\hbar_t^2 p^2 \left\|u_m''(\varsigma)\right\|_{[\varsigma_{t-1},\varsigma_{t+1}]},\ m=1,2.$$

   For

$$p_m = \min_{t=k_l,\ldots,k_r}\{p_{m,t}\} = \max_{t=k_l,\ldots,k_r}\left\{\sqrt{\frac{a_{mm}(\varsigma_t)+b_m(\varsigma_t)}{\epsilon}}, \sqrt{\frac{\delta b_m(\varsigma_t)}{\epsilon}}\right\}$$

   it follows from Lemmas 5 and 8 that

$$\left\|\boldsymbol{L}^N(\boldsymbol{U}-\boldsymbol{u})(\varsigma_t)\right\| \leq CN^{-2},\ t = k_l, \ldots, k_r.$$

□

Lemma 10. *The layer component $\boldsymbol{v}$ of the solution $\boldsymbol{\wp}$ and its discrete approximation $\boldsymbol{V}$ satisfies*

$$\left\|\boldsymbol{L}^N(\boldsymbol{V}-\boldsymbol{v})(\varsigma_t)\right\| \leq CN^{-2},\ t = 1, \ldots, N-1.$$

Proof.

1. When $t \in \{1, \ldots, k_l - 1\} \cup \{k_r + 1, \ldots, N - 1\}$, for the left side of the boundary layer portion, Taylor's expansion yields

$$\begin{aligned}\left\|\boldsymbol{L}_m^N(\boldsymbol{V}-\boldsymbol{v})(\varsigma_t)\right\| &= |(L_m - L_m^N)\boldsymbol{v}(\varsigma_t)| \\ &= \epsilon\frac{|\hbar_{t+1}^2 v_m'''(\phi_t^{(2)}) - \hbar_t^2 v_m'''(\phi_t^{(1)})|}{3(\hbar_{t+1}+\hbar_t)},\ m = 1, 2,\end{aligned}$$

   where $\phi_t^{(2)} \in (\varsigma_t, \varsigma_{t+1})$ and $\phi_t^{(1)} \in (\varsigma_{t-1}, \varsigma_t)$. Moreover,

$$\begin{aligned}|\hbar_{t+1}^2 v_m'''(\phi_t^{(2)})-\hbar_t^2 v_m'''(\phi_t^{(1)})| &\leq |\hbar_{t+1}^2-\hbar_t^2\|v_m'''(\phi_t^{(2)})|+\hbar_t^2|v_m'''(\phi_t^{(2)})-v_m'''(\phi_t^{(1)})| \\ &\leq C(|\hbar_{t+1}^2 - \hbar_t^2\|v_m'''(\varsigma_t)| + \hbar_t^2|\hbar_{t+1} + \hbar_t\|v_m^{(iv)}(\varsigma_t)|),\end{aligned}$$

where $|\phi_t^{(2)} - \phi_t^{(1)}| < (\hbar_{t+1} + \hbar_t)$. Now, using Lemmas 5 and 7 to compute

$$\begin{aligned}|\boldsymbol{L}^N(\boldsymbol{V}-\boldsymbol{v})(\varsigma_t)| &\le C\epsilon^{\frac{-1}{2}}\hbar_t^2 e^{\left(-\varsigma_t\sqrt{\frac{\zeta}{\epsilon}}\right)} + C\epsilon^{-1}\hbar_t^2 e^{\left(-\varsigma_t\sqrt{\frac{\zeta}{\epsilon}}\right)} \\ &\le C\gamma^2 N^{-2} \le CN^{-2}.\end{aligned}$$

Likewise, we can estimate the outcome for the right side of the boundary layer portion, and the desired result follows immediately.

2. When $t \in \{k_l, ..., k_r\}$, Taylor's expansion with integral remainder yields

$$\left\|\boldsymbol{L}_m^N(\boldsymbol{V}-\boldsymbol{v})(\varsigma_t)\right\| = |(L_m - L_m^N)\boldsymbol{v}(\varsigma_t)| \le C\epsilon \left\|v_m''(\varsigma)\right\|_{[\varsigma_{t-1},\varsigma_{t+1}]},\ m = 1, 2.$$

Now, using Lemma 5 yields the required bound

$$\left\|\boldsymbol{L}_m^N(\boldsymbol{V}-\boldsymbol{v})(\varsigma_t)\right\| \le C\begin{cases} e^{\left(-\varsigma_{t-1}\sqrt{\frac{\zeta}{\epsilon}}\right)}, & \varsigma_t \le \frac{1}{2}, \\ e^{\left(-(1-\varsigma_{t+1})\sqrt{\frac{\zeta}{\epsilon}}\right)}, & \varsigma_t > \frac{1}{2}. \end{cases}$$

For $t \ge k_l - 1$ and $\varsigma_t \le \frac{1}{2}$, Lemma (6) suggests

$$\left\|\boldsymbol{L}_m^N(\boldsymbol{V}-\boldsymbol{v})(\varsigma_t)\right\| \le Ce^{\left(-\varsigma_{k_l-1}\sqrt{\frac{\zeta}{\epsilon}}\right)} = C\left(e^{\left(\frac{-\varsigma_{k_l-1}}{2}\sqrt{\frac{\zeta}{\epsilon}}\right)}\right)^2 \le CN^{-2}.$$

□

We now summarize all the previously derived error estimates to present the main convergence result. The proof follows directly from Lemma 9, Lemma 10 and the triangle inequality.

Theorem 1. *Let $\boldsymbol{\wp}$ be the solution of* (2.1) *and $\boldsymbol{Y}$ be the solution of* (6.3) *Then, there exists a positive constant C independent of N and ϵ such that*

$$\|\boldsymbol{\wp} - \boldsymbol{Y}\|_{\bar{\Omega}_E^N} \le CN^{-2}.$$

8 Numerical experiments

In this section, we examine the performance of the proposed method using four model problems and present numerical findings. If the exact solution of the problem is unknown, we estimate the error $E_{m,\epsilon}^N$ using the double mesh principle [20], given by $E_{m,\epsilon}^N = \max\limits_{0\le t\le N} |Y_m^N(\varsigma_t) - \hat{Y}_m^{2N}(\hat{\varsigma}_2 t)|,\ m = 1, 2$. However, if the exact solution is available, we evaluate the maximum pointwise errors using the formula $E_{m,\epsilon}^N = \max\limits_{0\le t\le N} |Y_m^N(\varsigma_t) - \wp_m(\varsigma_t)|,\ m = 1, 2$. Here, $\wp_m(\varsigma_t)$ represents the exact solution, and $Y_m^N(\varsigma_t)$ denotes the numerical solution obtained at the grid points ς_t of the adaptive grid with N number of intervals. Moreover, we estimate the uniform errors using $E_m^N = \max\limits_{\epsilon\in K} E_{m,\epsilon}^N$

where $K = \{\epsilon | \epsilon = 2^0, 2^{-2}, ..., 2^{-40}\}$ and compute the order of convergence and parameter-uniform orders of convergence using

$$d^N_{m,\epsilon} = \log_2 \left(E^N_{m,\epsilon} / E^{2N}_{m,\epsilon} \right), \quad d^N_m = \log_2 \left(E^N_m / E^{2N}_m \right).$$

In the adaptive mesh generation process, we choose $Q = 1.3$. Tables 1–4 list the uniform errors and corresponding orders of convergence for the proposed method applied to Examples 1 and 2. The uniform errors decrease consistently as the number of grid intervals increases, and the orders of convergence are approximately two, confirming the second-order accuracy of the method. The results align with the theoretical predictions, reinforcing the method's effectiveness across different examples. For Example 3, Table 5 compares the maximum pointwise error and order of convergence using the proposed method and a hybrid finite difference method over a Shiskin mesh [33].

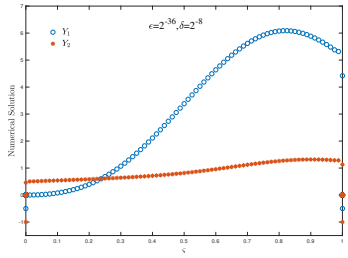

Figure 1. Numerical solution for Example 1 with $N = 160$.

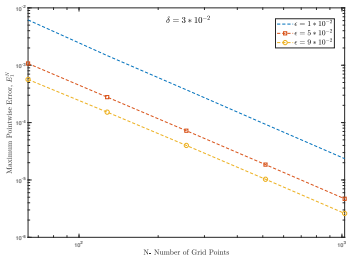

Figure 2. Comparison of maximum pointwise errors, E^N_1 for Example 1 for different values of ϵ.

Figure 1 illustrates the numerical solution of a system of second-order delay reaction-diffusion equations for Example 1 with $N = 160$, computed using the proposed difference scheme. The plot shows the behaviour of the numerical solution across the domain. The boundary layer effect is evident from the figure, highlighting the method's ability to capture steep gradients near the boundary. The solution remains stable and accurate, reflecting the robustness of the proposed scheme in handling the coupled system of delay reaction-diffusion equations. Figure 2 compares the maximum pointwise errors for various values of the perturbation parameter in Example 1.

Example 1. Consider the coupled system of singularly perturbed delay reaction diffusion boundary value problem for $\varsigma \in \Omega = (0, 1)$

$$-\epsilon \boldsymbol{\wp}''(\varsigma) + \begin{pmatrix} \varsigma^2 + e^{-2\varsigma} & -12\varsigma^2 \\ -\varsigma^3 & 4(1+\varsigma^4) \end{pmatrix} \boldsymbol{\wp}(\varsigma) + \begin{pmatrix} 2\varsigma^4 & 0 \\ 0 & \varsigma e^{-\varsigma} \end{pmatrix} \boldsymbol{\wp}(\varsigma - \delta) = \begin{pmatrix} \varsigma^4 \\ 2e^{\varsigma} \end{pmatrix},$$

where $\boldsymbol{\wp}(\varsigma) = \left(-\frac{\cos \varsigma}{2}, \varsigma - 1 \right)^T$ for $\varsigma \in [-\delta, 0]$ and $\boldsymbol{\wp}(1) = \left(-\frac{1}{2}, -1 \right)^T$.

The plot shows how the error varies with different values of perturbation parameter ϵ. The consistent pattern indicates the method's robustness to changes

Table 1. The errors E_m^N and orders of convergence d_m^N in approximations Y_m for Example 1 with $\epsilon = 2^{-4}$, $\delta = 2^{-6}$ and $m = 1, 2$.

	N=32	N=64	N=128	N=256	N=512	N=1024
E_1^N	8.372e-04	2.207e-04	5.768e-05	1.481e-05	3.757e-06	8.789e-07
d_1^N	1.96	1.98	1.99	1.99	1.99	
E_2^N	6.131e-03	1.546e-03	3.874e-04	9.689e-05	2.423e-05	6.057e-06
d_2^N	1.98	1.99	1.99	1.99	2.00	

Table 2. The errors E_m^N in approximations Y_m for Example 1 for different values of ϵ and N with $\delta = 0.03$ and $m = 1, 2$.

$\epsilon \downarrow$		N=32	N=64	N=128	N=256	N=512
0.01	E_1^N	1.160e-02	1.472e-03	3.727e-04	9.334e-05	2.353e-05
	E_2^N	5.057e-02	1.018e-02	2.411e-03	6.049e-04	1.514e-04
0.05	E_1^N	1.072e-03	2.777e-04	7.222e-05	1.852e-05	4.697e-06
	E_2^N	7.637e-03	1.931e-03	4.841e-04	1.211e-04	3.028e-05
0.09	E_1^N	5.642e-04	1.521e-04	3.998e-05	1.028e-05	2.609e-06
	E_2^N	4.273e-03	1.075e-03	2.691e-04	6.729e-05	1.682e-05

in ϵ, maintaining second-order accuracy across a range of perturbation sizes. Figure 3 shows the distribution of grid points for Example 2 with $N = 128$ emphasizing areas with higher density. The grid density is higher near the boundary layer, indicating that the adaptive algorithm effectively places more points where the solution requires higher resolution. This adaptive grid ensures better accuracy and efficiency in solving the problem.

Figure 4 depict a log-log plot of the maximum pointwise errors against the number of grid intervals for Example 2. The plot illustrates the error convergence rates for the two components of the solution. The linear behaviour in the log-log plot indicates second-order convergence, validating the theoretical error estimates provided in the paper. In contrast, Figure 5 compares the maximum pointwise error of the proposed method with a hybrid finite difference method over a Shiskin mesh for Example 3. The comparison demonstrates the superiority of the proposed hybrid spline difference method, which achieves lower maximum pointwise errors, particularly in resolving boundary layers. Finally, Figure 6 shows the comparison between the exact and numerical solutions for Example 4. The numerical solution closely matches the exact solution within and outside the boundary layer. This visual confirmation underscores the method's accuracy and reliability.

Example 2. Consider the coupled system of singularly perturbed delay reaction

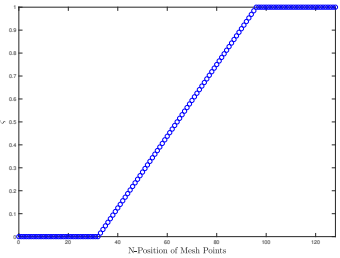

Figure 3. Density of grid points for Example 2 with $N = 128$.

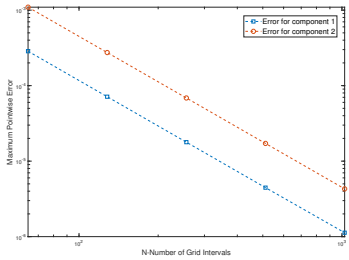

Figure 4. Loglog plot of maximum pointwise errors for Example 2.

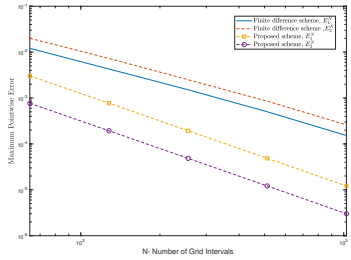

Figure 5. Comparison of maximum pointwise errors for Example 3 for proposed scheme with a finite difference scheme defined over a piecewise uniform Shishkin mesh.

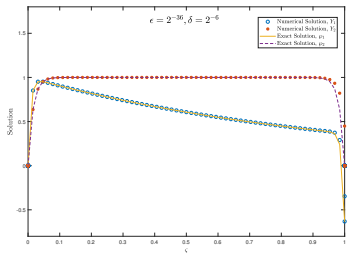

Figure 6. Comparison of numerical solution with the exact solution for Example 4 with $N = 128$.

diffusion boundary value problem for $\varsigma \in \Omega = (0, 1)$

$$-\epsilon \boldsymbol{\wp}''(\varsigma) + \begin{pmatrix} (\varsigma+1)^2 & -(1+\varsigma^3) \\ -2\cos\left(\frac{\pi\varsigma}{4}\right) & 3e^{-\varsigma} \end{pmatrix} \boldsymbol{\wp}(\varsigma) + \begin{pmatrix} \varsigma^2 & 0 \\ 0 & 10\varsigma \end{pmatrix} \boldsymbol{\wp}(\varsigma - \delta) = \begin{pmatrix} e^{\varsigma-1} \\ 4\varsigma \end{pmatrix},$$

where $\boldsymbol{\wp}(\varsigma) = \left(-\frac{\sin\varsigma}{2}, \varsigma\right)^T$ for $\varsigma \in [-\delta, 0]$ and $\boldsymbol{\wp}(1) = (0, 0)^T$.

Table 3. The errors E_m^N and orders of convergence d_m^N in approximations Y_m for Example 2 with $\epsilon = 2^{-4}$, $\delta = 2^{-6}$ and $m = 1, 2$.

	N=32	N=64	N=128	N=256	N=512	N=1024
E_1^N	1.147e-03	2.856e-04	7.133e-05	1.783e-05	4.456e-06	1.114e-06
d_1^N	2.00	2.00	2.00	2.00	2.00	
E_2^N	4.315e-03	1.094e-03	2.743e-04	6.864e-05	1.716e-05	4.292e-06
d_2^N	1.97	1.99	1.99	2.00	1.99	

Table 4. The errors E_m^N in approximations Y_m for Example 2 for different values of ϵ and N with $\delta = 0.03$ and $m = 1, 2$.

$\epsilon \downarrow$		N=32	N=64	N=128	N=256	N=512
0.01	E_1^N	1.065e-02	1.928e-03	4.464e-04	1.115e-04	2.786e-05
	E_2^N	3.405e-02	7.115e-03	1.704e-03	4.283e-04	1.072e-04
0.05	E_1^N	1.435e-03	3.571e-04	8.916e-05	2.228e-05	5.571e-06
	E_2^N	5.367e-03	1.365e-03	3.428e-04	8.580e-05	2.146e-05
0.09	E_1^N	7.954e-04	1.983e-04	4.953e-05	1.238e-05	3.095e-06
	E_2^N	3.014e-03	7.606e-04	1.906e-04	4.767e-05	1.192e-05

Example 3. Consider the coupled system of singularly perturbed delay reaction diffusion boundary value problem

$$-\epsilon \boldsymbol{\wp}''(\varsigma) + \begin{pmatrix} 11 & 0 \\ 0 & 16 \end{pmatrix} \boldsymbol{\wp}(\varsigma) + \begin{pmatrix} -(\varsigma^2+1) & -(\varsigma+1) \\ -\varsigma & -\varsigma \end{pmatrix} \boldsymbol{\wp}(\varsigma-1) = \begin{pmatrix} e^{\varsigma} \\ e^{\varsigma} \end{pmatrix},$$

where $\boldsymbol{\wp}(\varsigma) = (1,1)^T$ for $\varsigma \in [-1, 0]$ and $\boldsymbol{\wp}(1) = (1,1)^T$.

Table 5. Comparison of maximum pointwise errors E_m^N and order of convergence d_m^N for Example 3 of the proposed scheme with a hybrid difference scheme on a Shiskin mesh [33] with $m = 1, 2$.

N	Method in [33]		Proposed method		Method in [33]		Proposed method	
	E_1^N	d_1^N	E_1^N	d_1^N	E_2^N	d_2^N	E_2^N	d_2^N
32	2.8268e-2	1.2217	1.154e-02	1.9240	4.4596e-2	1.1560	3.002e-03	1.9650
64	1.2121e-2	1.5008	3.041e-03	1.9788	2.0012e-2	1.4547	7.689e-04	1.9912
128	4.2829e-3	1.5013	7.715e-04	1.9945	7.3012e-3	1.5440	1.934e-04	1.9976
256	1.5128e-3	1.5937	1.936e-04	1.9988	2.5038e-3	1.5529	4.843e-05	1.9997
512	5.0124e-4	1.7179	4.844e-05	1.9996	8.5338e-4	1.7106	1.211e-05	2.0074
1024	1.5237e-4		1.212e-05		2.6074e-4		3.012e-06	

Example 4. Consider the coupled system of singularly perturbed delay reaction diffusion boundary value problem for $\varsigma \in \Omega = (0, 1)$

$$-\epsilon \boldsymbol{\wp}''(\varsigma) + \begin{pmatrix} 2(\varsigma+1)^2 & -\varsigma^2 \\ -\sin(\pi\varsigma) & e^{1-\varsigma} \end{pmatrix} \boldsymbol{\wp}(\varsigma) + \begin{pmatrix} \varsigma^2 & 0 \\ 0 & \varsigma \end{pmatrix} \boldsymbol{\wp}(\varsigma-\delta) = \boldsymbol{g}(\varsigma),$$

where $\boldsymbol{\wp}(\varsigma) = \big(\varsigma, \sin(\varsigma)\big)^T$ for $\varsigma \in [-\delta, 0]$ and $\boldsymbol{\wp}(1) = \Big(e^{-1} - 1, 0\Big)^T$. Here, the function $\boldsymbol{g}(\varsigma) = (g_1(\varsigma), g_2(\varsigma))^T$ is such that the exact solution of the problem is $\wp_1(\varsigma) = (\varsigma-1)e^{-\frac{2\varsigma}{\epsilon+\delta}} - \varsigma e^{-\frac{2(1-\varsigma)}{\epsilon+\delta}} + e^{-\varsigma}$ and $\wp_2(\varsigma) = (\varsigma-1)e^{-\frac{\varsigma}{\epsilon+\delta}} - \varsigma e^{-\frac{1-\varsigma}{\epsilon+\delta}} + 1$.

9 Conclusions

A novel uniformly accurate difference scheme specifically designed for solving a coupled system of singularly perturbed delay reaction-diffusion equations on an equidistributed grid is presented in this work. This adaptive grid leverages the equidistribution of a positive monitor function, which is a linear combination of a constant floor and a power of the second derivative of the solution. The difference scheme combines an exponential spline difference scheme for the outer layer and a cubic spline difference scheme for the boundary layer on the adaptive mesh generated. This innovative approach enhances the accuracy of the numerical solutions and maintains computational efficiency. We performed a rigorous theoretical analysis. Our numerical experiments validate the uniform convergence and theoretical findings, demonstrating the method's robustness regardless of the perturbation parameter size.

Acknowledgements

This document is the result of the research project MTR/2021/000117 funded by Science and Engineering Research Board, Department of Science & Technology, Government of India.

References

[1] Aakansha, S. Kumar and H. Ramos. A rapidly converging domain decomposition algorithm for a time delayed parabolic problem with mixed type boundary conditions exhibiting boundary layers. *Journal of Applied Mathematics and Computing*, **70**(2):1043–1067, 2024. https://doi.org/10.1007/s12190-024-01987-8.

[2] N.S. Bakhvalov. On the optimization of methods for solving boundary value problems with boundary layers. *Zh. Vychisl. Mat. Mat. Fis.*, **9**:1969, 841–859.

[3] L. Barbu and G. Moroşanu. *Singularly Perturbed Boundary Value Problems*. Birkhäusar, Basel, 2007.

[4] P. Das. Comparison of a priori and a posteriori meshes for singularly perturbed nonlinear parameterized problems. *Journal of Computational and Applied Mathematics*, **290**:16–25, 2015. https://doi.org/10.1016/j.cam.2015.04.034.

[5] P. Das and S. Natesan. Higher-order parameter uniform convergent schemes for Robin type reaction-diffusion problems using adaptively generated grid. *International Journal of Computational Methods*, **9**(04):1250052, 2012. https://doi.org/10.1142/S0219876212500521.

[6] Z. Gajic and M.T. Lim. *Optimal Control of Singularly Perturbed Linear Systems and Applications*. Marcel-Dekker, New York, 2001. https://doi.org//10.1201/9780203907900.

[7] E.C. Gartland. Graded mesh difference schemes for singularly perturbed two point boundary value problems. *Mathematics of Computation*, **51**:631–657, 1988. https://doi.org/10.1090/S0025-5718-1988-0935072-1.

[8] A. Gupta and A. Kaushik. A higher-order accurate difference approximation of singularly perturbed reaction-diffusion problem using grid equidistribution. *Ain Shams Engineering Journal*, **12**(4):4211–4221, 2021. https://doi.org/10.1016/j.asej.2021.04.024.

[9] A. Gupta and A. Kaushik. A robust spline difference method for robin-type reaction-diffusion problem using grid equidistribution. *Applied Mathematics and Computation*, **390**:125597, 2021. https://doi.org/10.1016/j.amc.2020.125597.

[10] A. Gupta and A. Kaushik. A higher-order hybrid finite difference method based on grid equidistribution for fourth-order singularly perturbed differential equations. *Journal of Applied Mathematics and Computing*, **68**(2):1163–1191, 2022. https://doi.org/10.1007/s12190-021-01560-7.

[11] A. Gupta, A. Kaushik and M. Sharma. A higher-order hybrid spline difference method on adaptive mesh for solving singularly perturbed parabolic reaction–diffusion problems with robin-boundary conditions. *Numerical Methods for Partial Differential Equations*, **39**(2):1220–1250, 2023. https://doi.org/10.1002/num.22931.

[12] A. Kaushik, A. Gupta, S. Jain, Ş. Toprakseven and M. Sharma. An adaptive mesh generation and higher-order difference approximation for the system of singularly perturbed reaction–diffusion problems. *Partial Differential Equations in Applied Mathematics*, **11**:100750, 2024. https://doi.org/10.1016/j.padiff.2024.100750.

[13] A. Kaushik, V. Kumar, M. Sharma and N. Sharma. A modified graded mesh and higher order finite element method for singularly perturbed reaction–diffusion problems. *Mathematics and Computers in Simulation*, **185**:486–496, 2021. https://doi.org/10.1016/j.matcom.2021.01.006.

[14] A. Kaushik, A.K. Vashishtha, V. Kumar and M. Sharma. A modified graded mesh and higher order finite element approximation for singular perturbation problems. *Journal of Computational Physics*, **395**:275–285, 2019. https://doi.org/10.1016/j.jcp.2019.04.073.

[15] J. Kevorkian and J.D. Cole. *Perturbation Methods in Applied Mathematics*. Springer, Berlin, 2013. https://doi.org/10.1007/978-1-4757-4213-8.

[16] N. Kopteva, N. Madden and M. Stynes. Grid equidistribution for reaction–diffusion problems in one dimension. *Numerical Algorithms*, **40**(3):305–322, 2005. https://doi.org/10.1007/s11075-005-7079-6.

[17] N. Kopteva and M. Stynes. A robust adaptive method for a quasi-linear one-dimensional convection-diffusion problem. *SIAM Journal on Numerical Analysis*, **39**(4):1446–1467, 2001. https://doi.org/10.1137/S003614290138471X.

[18] K. Kumar, P.C. Podila, P. Das and H. Ramos. A graded mesh refinement approach for boundary layer originated singularly perturbed time-delayed parabolic convection diffusion problems. *Mathematical Methods in the Applied Sciences*, **44**(16):12332–12350, 2021. https://doi.org/h10.1002/mma.7358.

[19] T. Linß. Uniform pointwise convergence of finite difference schemes using grid equidistribution. *Computing*, **66**(1):27–39, 2001. https://doi.org/10.1007/s006070170037.

[20] T. Linß. *Layer Adapted Meshes for Reaction Convection Diffusion Problems*. Springer, Berlin, 2010.

[21] P.C. Lu. *Introduction to the Mechanics of Viscous Fluids*. Holt-Rinehart & Winston, New York, 1973.

[22] N. Madden and M. Stynes. A uniformly convergent numerical method for a coupled system of two singularly perturbed linear reaction-diffusion problems. *IMA Journal of Numerical Analysis*, **23**(4):627–644, 2003. https://doi.org/10.1093/imanum/23.4.627.

[23] J.J.H. Miller. *Singular Perturbation Problems in Chemical Physics*. John Wiley & Sons, New York, 1997. https://doi.org/10.1002/9780470141564.

[24] J.D. Murray. *Mathematical Biology II: Spatial models and biomedical applications*, volume 3. Springer,New York, 2001.

[25] A.H. Nayfeh. *Perturbation Methods*. Wiley, New York, 1979.

[26] R.E. O'Malley. *Introduction to Singular Perturbations*. Academic Press, New York, 1974.

[27] K.C. Patidar and K.K. Sharma. ε-uniformly convergent non-standard finite difference methods for singularly perturbed differential difference equations with small delay. *Applied Mathematics and Computation*, **175**(1):864–890, 2006. https://doi.org/10.1016/j.amc.2005.08.006.

[28] S. Priyadarshana, J. Mohapatra and H. Ramos. Robust numerical schemes for time delayed singularly perturbed parabolic problems with discontinuous convection and source terms. *Calcolo*, **61**(1):1, Nov 2023. https://doi.org/10.1007/s10092-023-00552-2.

[29] M.H. Protter and H.F. Weinberger. *Maximum Principles in Differential Equations*. Springer-Verlag, New York, 1984. https://doi.org/10.1007/978-1-4612-5282-5.

[30] S. Saini, P. Das and S. Kumar. Computational cost reduction for coupled system of multiple scale reaction diffusion problems with mixed type boundary conditions having boundary layers. *Revista de la Real Academia de Ciencias Exactas, Físicas y Naturales. Serie A. Matemáticas*, **117**(2):66, 2023. https://doi.org/10.1007/s13398-023-01397-8.

[31] S. Saini, P. Das and S. Kumar. Parameter uniform higher order numerical treatment for singularly perturbed robin type parabolic reaction diffusion multiple scale problems with large delay in time. *Appl. Numer. Math.*, **196**:1–21, 2024.

[32] D. Shakti, J. Mohapatra, P. Das and J. Vigo-Aguiar. A moving mesh refinement based optimal accurate uniformly convergent computational method for a parabolic system of boundary layer originated reaction–diffusion problems with arbitrary small diffusion terms. *Journal of Computational and Applied Mathematics*, **404**:113167, 2022. https://doi.org/10.1016/j.cam.2020.113167.

[33] V. Subburayan and N. Ramanujam. An initial value method for singularly perturbed system of reaction-diffusion type delay differential equations. *Journal of the Korean Society for Industrial and Applied Mathematics*, **17**(4):221–237, 2013. https://doi.org/10.12941/JKSIAM.2013.17.221.

[34] R. Vulanović and L. Teofanov. A modification of the Shishkin discretization mesh for one-dimensional reaction-diffusion problems. *Applied Mathematics and Computation*, **220**:104–116, 2013. https://doi.org/10.1016/j.amc.2013.05.055.